Determining the Dynamic Properties of Spruce Wood Using the Taylor Anvil Test

Miroslav Jopek,[a] Radek Ridky,[b] Pavel Kral,[c] Tomas Pipiska,[c] Jozef Rahel,[c] Roman Reh,[d] and Lubos Kristak [d]

Spruce wood is one of the most widely used materials in the production of lightweight wood-based composites in central Europe. The quality, weight, and geometric parameters of wood chips have a significant impact on the resulting quality of the manufactured composite product. Numerical simulations are necessary for advanced optimization of the quality of composite components and the manufacturing process itself. These simulations require adequate input material data and a model to produce results applicable to the output of industrial practice. In this study, a material model for spruce wood was established using the Taylor anvil test (TAT). This, in contrast to the commonly used Hopkinson compression test, corresponds better to the actual loading process. A new measurement method for shock pulses was developed to implement TAT obtained data for a realistic material model. The method was compared with numerical simulations in Ansys LS DYNA. Based on the results, parameters for the Johnson-Cook equation were determined, which can be applied in the production of disintegrations and, consequently, in the dynamic loading of spruce composite materials.

DOI: 10.15376/biores.19.2.3725-3739

Keywords: Taylor anvil test; Johnson-Cook; LS DYNA; Norway spruce; Dynamic characteristics

*Contact information: a: Brno University of Technology, Technicka 2, 616 69 Brno-Kralovo pole, Czech Republic; b: SVS FEM s.r.o., Trnkova 3104/117c, 628 00 Brno-Lisen, Czech Republic; c: Mendel University in Brno, Zemedelska 1665/1, 613 00 Brno-sever Cerna Pole, Czech Republic; d: Faculty of Wood Science and Technology, Technical University in Zvolen, T.G. Masaryka 24, 960 01 Zvolen, Slovakia; * Corresponding author: jopek@fme.vutbr.cz*

INTRODUCTION

Spruce wood is one of the most widespread coniferous tree species in Europe. According to the Report on the State of Europe's Forests, the area covered by forests in 2020 was 34,983 million hectares, of which spruce accounted for 23%. (Forest Europe 2020). Given these facts, spruce is also among the most widely used wood materials for the production of composite particleboards, OSB, and others. One of the progressive ways to optimize the production of composite particleboard is to use numerical methods. In any numerical simulation software, it is necessary to specify the material itself and describe it using a suitable material model, with constitutive equations.

Several material models that employ constitutive equations are known, such as Mat143 wood, Johnson-Cook, Zerelli-Armstrong, *etc*. (Jopek 2021; Kruszka and Sobczyk 2022). The selection of a specific material model always depends on the type of material for which the constitutive equations are applicable (Lipinski 2023). Wood, by its nature, is an orthotropic material, which means that the constitutive equation must account for anisotropy and different mechanical properties in three mutually perpendicular directions

(Sebek *et al*. 2021). Current research on high-dynamic strains of organic materials involves studies of epoxy matrix composite materials (White *et al*. 2009), deformation of polymeric materials (Shin *et al*. 2008), and the behavior of wood for the production of composite boards, such as pine, beech, and others (Buchar *et al*. 2000). The description of the orthotropic properties, especially of spruce and timber, is addressed by Zulkiffi, who utilizes the material model MAT 026 to describe the properties of spruce wood, where the test specimen is modeled as a Honeycomb. Numerical simulation with Mat 026 is compared with experiments under quasi-static conditions and subsequently under dynamic conditions conducted using a Hopkinson split bar (Zulkifli *et al*. 2021). The simulation analysis of the circular sawing process of medium density fiberboard, which approximates the process of disintegration, was carried out by Yu *et al*. (2023). For the numerical simulation of the sawing process, a modified Johnson-Cook equation was used, and the results were then compared with the author's own experiment of the cutting process. As input data for determining the coefficients of the J-C equation, an experiment conducted using a Hopkinson split bar was used.

The presence of lignin and other polymeric components in wood can also lead to viscous behavior, where wood deforms over time and exhibits a negative sensitivity to the strain rate, *i.e.* true stress decreases with strain rates (Pettersen 1984). However, the negative influence on the strain rate in wood is a matter of further research, as the testing method using a Hopkinson split bar is typically performed in the range of strain rates from 500 up to 3000 s^{-1} (Palamidi and Harrigan 2006; Holmgren *et al*. 2008; Moilanen *et al*. 2016). For higher strain rates up 6000 s^{-1}, it is necessary to use other testing devices and evaluation methods. One option is to use equipment utilizing the Taylor anvil test (TAT), as it reaches impact speeds of up to 250 m/s at a strain rate up 10^5 s^{-1} (Taylor 1948). Unfortunately, with the TAT testing device or respective evaluation methodology, it is not possible to utilize the assumptions of uniaxial stress state or propagation of uniaxial stress pulses (initiation, reflected, and transmitted) as with the Hopkinson split bar. Rather, one has to utilize the comparison of results (geometric and force) of the TAT experiment with numerical simulation described using constitutive equations. In the present case, a modified constitutive equation J-C, was used. It describes, among other things, the sensitivity to strain rate, which is important for determining the positive or negative influence of the material on the strain rate.

In this respect, the dynamic test using the TAT is the only method that employs direct impact loading of the specimen, where high values of dynamic pressures are required. In addition, this loading occurs within a very short time interval, mimicking the actual process of achieving the production of composite components through disintegration. The method's principle involves shooting a test specimen with an initial diameter d_0 and initial length L_0 onto a rigid plate (rod), as shown in Fig. 1a.

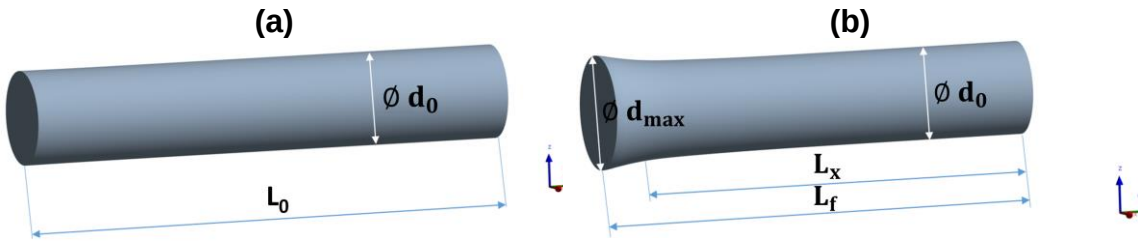

Fig. 1. Test specimen TAT: before TAT (a); after TAT (b)

The typical impact speed of the specimen ranges from 30 to 240 m/s. After impact on the rigid plate, the material deforms (destroyed) to a final length L_f, with the undeformed portion of the specimen having a length of L_x. For non-destroyed materials, it is also possible to identify the maximum final diameter d_{max} of the specimen on the impact side – see Fig. 1b.

EXPERIMENTAL

The study was conducted in two steps. At first, experiments were carried out with spruce wood under quasi-static conditions. The TAT apparatus was used to approximate as closely as possible the actual disintegration in the production of wood strands. The acquired experimental data was consequently cross-correlated with the numerical simulations. The numerical simulation for the TAT of spruce wood were aimed primarily at determining individual parameters of the modified J-C constitutive equation. The agreement between the experimental and numerically simulation made it possible to determine critical materials parameters of the spruce wood with a sufficient degree of confidence. These parameters will find their use in subsequent numerical simulations of dynamic loading processes in spruce wood, especially in disintegration technology.

The test specimens of Norway spruce (*Picea abies*) for TAT and for quasi-static tests were obtained from trees aged between 25 and 30 years. Specimens were selected for testing that exhibited no defects of either natural or mechanical nature. The trees were harvested during the dormant period (February - March) to preserve their natural moisture, and subsequently, the semi-finished products were stored in a cooling device at a constant temperature of 2°C. The density of individual specimens made from 10×10 mm rectangular bars ranged from 489 to 558 kg/m^3 and were cut at a distance of approximately 500 mm from the tree trunk. The moisture content of the specimens ranged from 57 to 62%. This moisture content was measured after the experiment using the oven-drying (gravimetric) method at a drying temperature of 100 °C (212 °F).

Taylor Anvil Test (TAT) Experiment

The TAT experiment was performed using a pneumatic gun. A schematic representation of the apparatus is shown in Fig. 2.

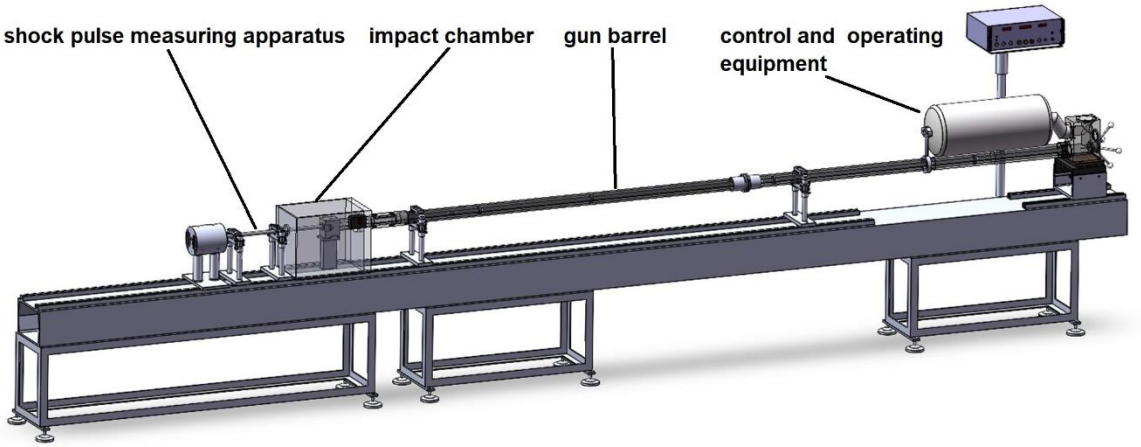

Fig. 2. Schematic representation of the experimental setup of TAT

The test specimen, with a length of L_0 = 40 mm and a diameter of d_0 = 10 mm, was lathed from rectangular bars and subsequently mechanically ground into a cylindrical shape with an accuracy of ± 0.1 mm. Before the TAT experiment, the dimensions of specimen were measured using a SOMET micrometer (Somet CZ, Bílina, Czech Republic) and weighed on a laboratory scale TSCALE NHB 150+ (T-SCALE, Taipei, China). A single cylindrical specimen was then loaded into a specially designed 3D printed capsule, which ensures its perpendicular impact onto the impactor. The impactor consisted of a MARAGING 350 steel rod with four strain gauges (HBM, HBK, Darmstadt, Germany) attached to its circumference in a Wheatstone bridge configuration. These strain gauges were used to measure and record voltage pulses generated by the impact of the test specimen on the rod. On the opposite side of the impactor, the rod was in contact with a KISTLER dynamometer 9363A (Kistler, Winterthur, Switzerland), which measured the impact force of the test specimen, recorded on a Tektronix digital oscilloscope TDS 210. The impact of the test specimen onto the impactor rod was further recorded using a high-speed camera Photron Fastcam SA-X2 (Photron, Tokyo, Japan). To capture the complete geometry of the test specimen, image analysis was performed using the NIS-Elements software (Nikon Instruments, Tokyo, Japan) and an Imaging Source camera (Imaging Source, Regensburg, Germany).

Numerical Simulation

For the TAT numerical simulation, the ANSYS - LS DYNA 3D (Ansys, Canonsburg, Pennsylvania, USA) was used. A hexagonal mesh with 711 157 elements and 730 542 nodes was defined for the cylindrical specimen. In the numerical simulation of the TAT, the specifications included no remeshing but erroring used. The temperature was set to match the experimental temperature, *i.e.* 23 °C. The modified Johnson-Cook constitutive equation, and the J-C equation for failure were used. To determine the parameters and coefficients of the J-C equation, quasi-static compression tests, quasi-static bending tests and shear tests were performed in addition to TAT. A detailed description of the J-C constitutive equation and experimental procedures is beyond the scope of this article, but can be found elsewhere (Cook and Johnson 1985). For orthotropic materials such as spruce wood, a simplified modified Johnson-Cook constitutive equation for failure (Khare *et al.* 2021), which does not consider the effect of temperature on strain resistance, states that:

$$\varphi_f = \left[D_1 + D_2 \cdot exp\left(D_3 \cdot \frac{\sigma_m}{\sigma_{ef}}\right)\right] \cdot \left[1 + D_4 \cdot ln\frac{\dot{\varphi}}{\dot{\varphi}_0}\right]$$

where φ_f denotes strain at the failure, $D_1 - D_4$ are failure parameters, σ_m [MPa] is average value of the three normal stress components, σ_{ef} [MPa] is equivalent stress, $\dot{\varphi}$ [s^{-1}] is the strain rate, and $\dot{\varphi}_0$ [s^{-1}] represents the reference strain rate.

RESULTS AND DISCUSSION

Quasi-static Compression Test

To determine the parameters and coefficients under quasi-static conditions for the modified J-C, a quasi-static compression test of spruce wood was carried out on the ZD 40 testing machine. The compression speed was set at 0.16 mm/s, and the average strain rate reached values of 0.017 s^{-1}. As can be seen in Fig. 3, there was a significant increase in

stress up to 18.2 MPa with an actual strain value of 0.035, followed by a gradual decrease in stress to 4 MPa with an actual strain value of 0.5 due to failure, *i.e.* specimen destruction.

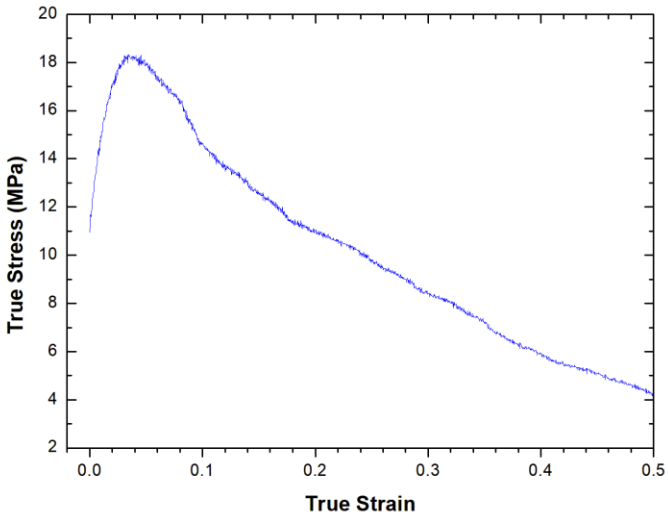

Fig. 3. The stress-strain curve for spruce wood at a strain rate of 0.017 s^{-1}

Compression Test *via* TAT

To determine the dynamic parameters and coefficients J-C, the TAT test was performed. In contrast to the quasi-static tests, where the dependence of the actual stress on the actual strain was evaluated directly from the measuring and evaluation apparatus, in the dynamic compression test using TAT, a detailed analysis of the experiments was evaluated and performed. The procedures were carried out starting from image analysis, through the evaluation of the deformation process by means of a high-speed camera, impact force measurements, pressure pulse waveform on the impact rod, to the comparison of the TAT experimental results (force, stress pulses, and specimen geometry) with numerical simulations.

Image analysis and geometry of the TAT specimen

The geometry of the spruce wood test specimen before TAT is shown in Fig. 4a. Figure 4b shows the deformed spruce wood test specimen after TAT with an impact speed of 144.5 m/s; Fig. 4c illustrates the process of capturing the resulting contour of that specimen using an Imaging Source camera and NIS Elements software. This contour was parametrized and exported from the NIS-Elements software to a spreadsheet.

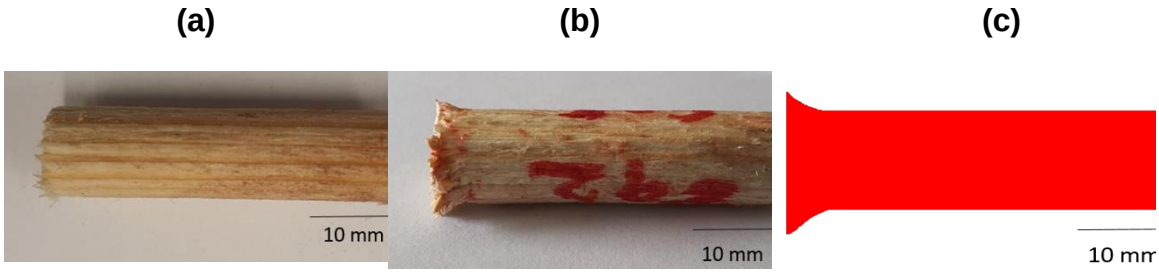

Fig. 4. (a) Test specimen of spruce wood before TAT; (b) test specimen of spruce wood after TAT - impact speed 144.5 m/s; (c) captured contour of the test specimen after TAT

High-speed camera capture of specimen deformation

Figure 5 shows an illustrative example of the temporal evolution of the deformation profile of a spruce wood test specimen at an impact velocity of 197.6 m/s. The camera was set to 100,000 fps, which appears to be the minimum required for contour change identification. The images clearly show the central impact on the impactor rod. Figure 5a displays the test specimen at the moment of impact on the impact rod at an impact speed of 197.6 m/s. Figure 5b show the progression of plastic deformation at 10 µs after impact and Figs. 5c and 5d failure of the destroyed spruce wood test specimen at 60 and 90 µs after impact to the impact rod.

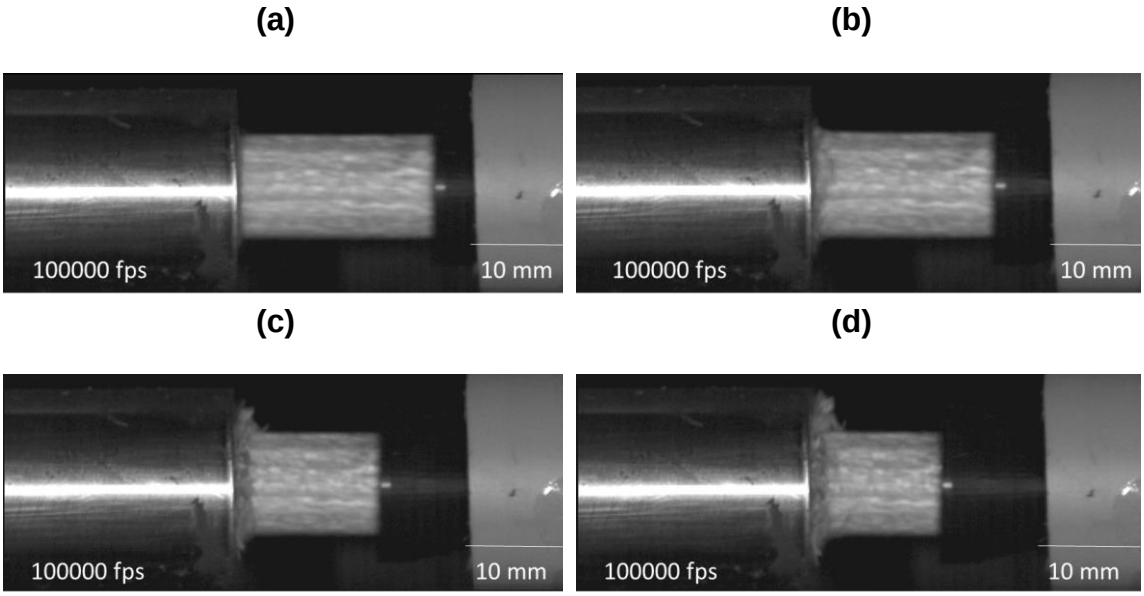

Fig. 5. Spruce wood test specimen at an impact speed of 197.6 m/s: (a) upon contact with the impact surface; (b) 10 µs after impact; (c) 60 µs after impact; (d) 90 µs after impact

Impact Force

The material response to impact forces was determined by evaluating the stress pulse profiles, as shown in Fig. 6, for two different impact speeds of 144.5 m/s and 197.6 m/s.

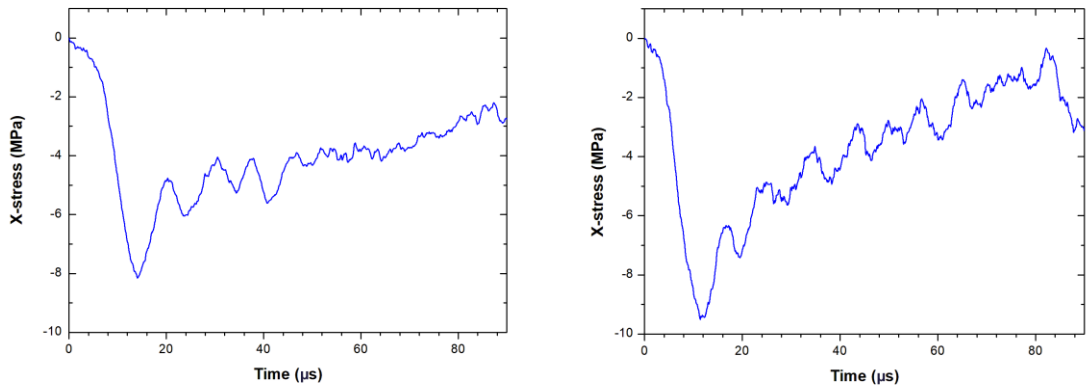

Fig. 6. The stress pulse on the impact rod - impact speed 144.5 m/s (a); (b) impact speed 197.6 m/s

Initially, there was a sharp increase in stress, followed by oscillations and subsequent damping. Comparison of the stress pulses reveals that as the impact speed of the test specimen on the rod increased, the duration of the stress pulse decreased. In these cases, the pulse duration decreased from 120 to 84 µs. A similar trend was observed in the stress pulse, where the peak stress increased with increasing impact speed.

To verify these experimental data, the actual impact force was measured using a Kistler dynamometer. Figure 7a shows that the maximum impact force for the specimen with an impact speed of 144.5 m/s reaches a maximum value of 2.5 kN. The duration of the impact force corresponded to the length of the stress pulse recorded on the rod, which was 120 µs. For the specimen with an impact speed of 197.6 m/s, the maximum impact force was 3.5 kN (Fig. 7b). The duration of the impact force matches the duration of the stress pulse applied to the impactor rod, which was 84 µs.

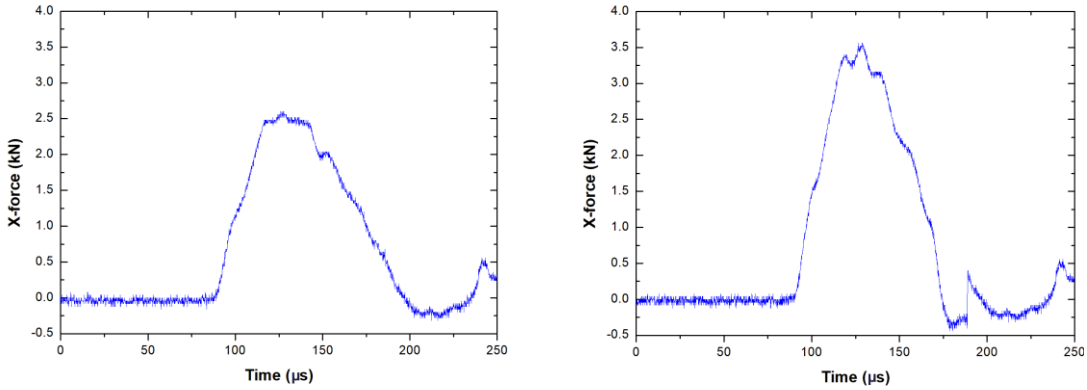

Fig. 7. The profile of the impact force: (a) impact speed 144.5 m/s; (b) impact speed 197.6 m/s

FEM analysis for J-C material model

Figure 8 (a) shows the contour of the test specimen at an impact speed of 144.5 m/s at a time of 100 µs after the impact, following the final optimization of the parameters of the J-C equation. From the numerical simulation, it can be observed that the specimen experiences failure, primarily on the front face of the test specimen, where the displayed x-stress within the specimen reaches its maximum value.

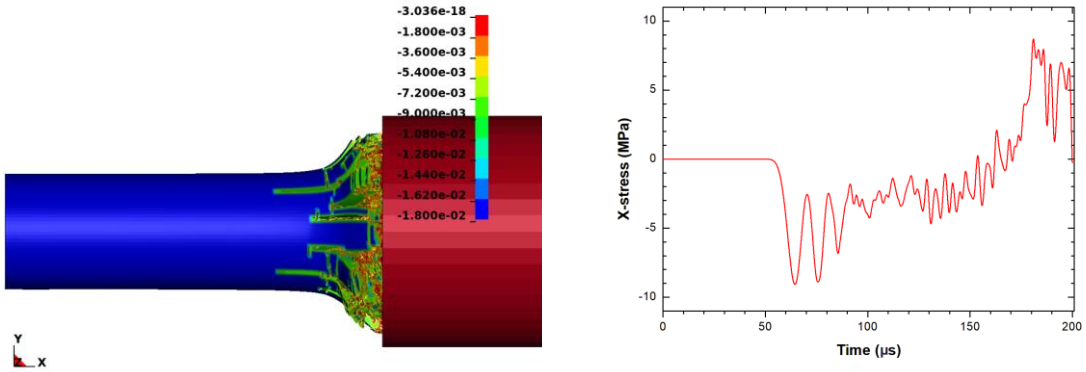

Fig. 8. (a) Geometry contour of the test specimen at an impact speed of 144.5 m/s at a time of 100 µs after impact. (b) Results of the numerical simulation of the stress pulse waveform on the impact rod caused by the impact of the test specimen at an impact speed of 144.5 m/s (b)

The calculated stress pulse profile on the rod is plotted in Fig. 8b. The initial stress wave offset by approximately 50 μs can be attributed to the setup of the boundary conditions in the numerical simulation, where the test specimen is not in direct contact with the test rod before the impact, similarly to the real experiment. However, at the impact speed of 144.5 m/s, the duration of the stress pulse matched the experimentally observed value of 120 μs.

Based on all the experiments mentioned above, from quasi-static compression tests to dynamic TAT tests in which the geometrical parameters of the test specimens, impact forces and pulse on the impact bar were measured, were compared with numerical simulations of TAT. Based on the best agreement between the TAT experiments and the TAT numerical simulations, the coefficients and constants of the J-C material model have been determined as listed in Tables 1 and 2.

Table 1. Parameters of Developed Johnson-Cook Constitutive Equation

Parameter	*A* [MPa]	*B* [MPa]	*C* [-]	*n* [-]
Value	10.95	30.59	0.01	0.43

Table 2. Parameters of Developed Johnson-Cook Failure Constitutive Equation

Parameter		D_1 [-]	D_2 [-]	D_3 [-]	D_4 [-]	σ_m/σ_{ef} [-]
Value		0.025	0.197	-0.084	-0.015	-9.039

Figure 9 shows the stress-strain relationship from evaluated data involving the J-C equation from Table 1. For illustrative purposes, three strain rates were selected: 0.017, 1200, and 10,000 s^{-1}.

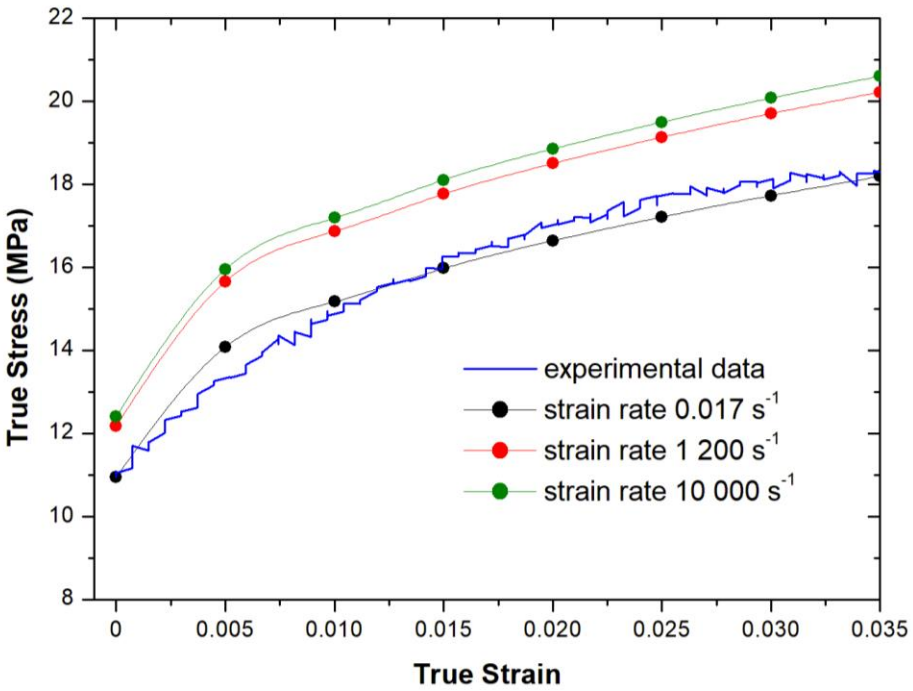

Fig. 9. The dependence of true stress on true strain for spruce wood - comparison of the experiment and obtained Johnson-Cook parameters through numerical simulation for various strain rates

Fig. 10. Detail of the spruce specimen (a) and disintegrated strands (b) at knife ring flaker MRZ 1400

The results of the numerical simulation of the disintegration process with the determined J-C parameters from Table 1, Table 2, and Fig. 9, are shown in Fig. 11.

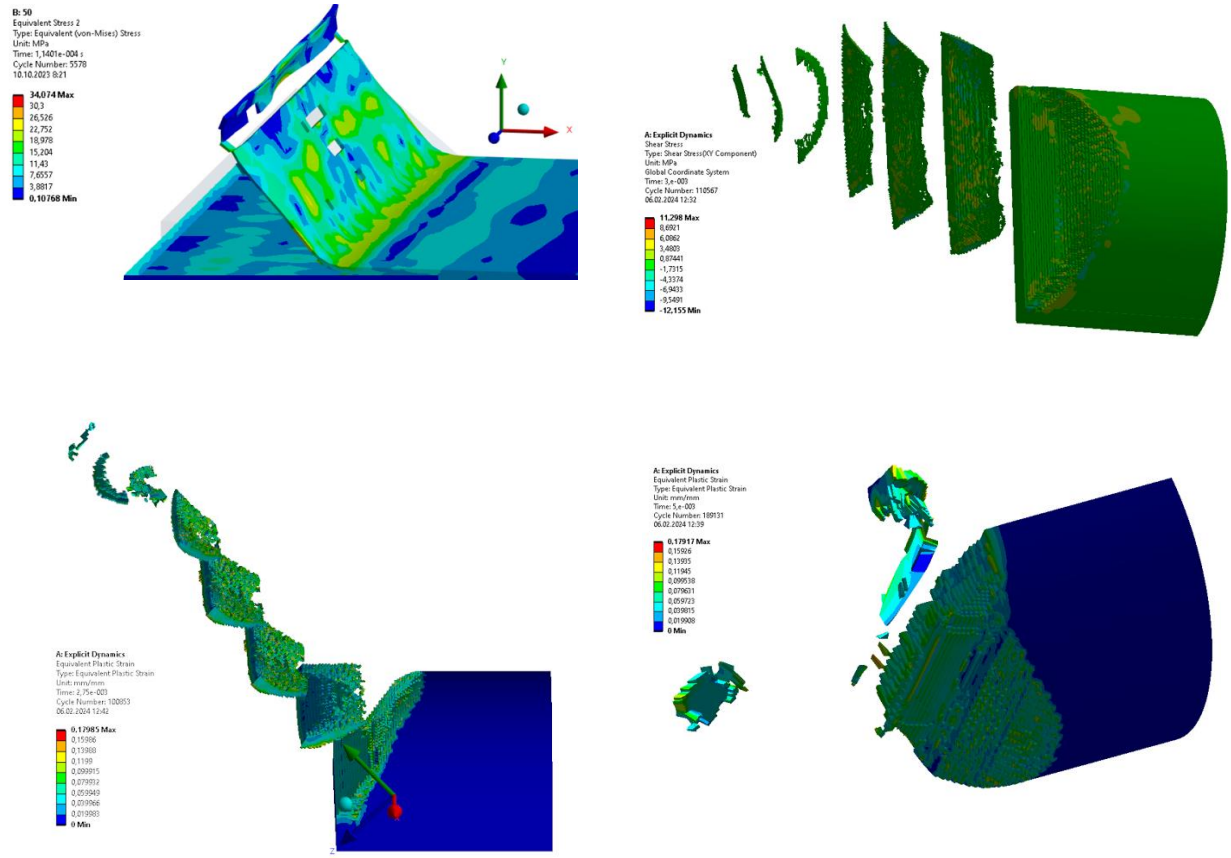

Fig. 11. Disintegration process of spruce wood using FEM – Ansys and J-C constitutive equation

Strain rate 0.017 s^{-1} represents material model under quasi-static condition, strain rate 1200 s^{-1} represents stress-strain curve under dynamic conditions, *e.g.* mean strain rate by Hopkinson split bar test, and strain rate 10,000 s^{-1} represents material model under dynamic conditions, *e.g.* TAT test. It is evident from the graph that the proposed parameters of the J-C constitutive equation correspond well with the results of the experimental quasi-static compression test. At higher strain rates, including very high strain rates, a curve shift occurs due to the sensitivity of the material to the strain rate. It can be seen that the spruce wood to strain 0.035 did not exhibit negative strain rate sensitivity.

In the comparison of experiment results from the disintegration process with numerical simulation outcomes for the aforementioned material model, geometric parameters of disintegrated particles were analysed in relation to the settings on the knife ring flaker OSB - MRZ 1400 (Dieffenbacher GmbH, Eppingen, Germany). The resulting shapes and dimensions of the input semi-finished product, as well as the disintegrated particles, are illustrated in Fig. 10.

During the experimental disintegration process, the quantity and shape of disintegrated particles, as well as the maximum thickness, length, and width of the disintegrated particles for the measured input semi-finished product, were quantified. This is evident from Fig. 12.

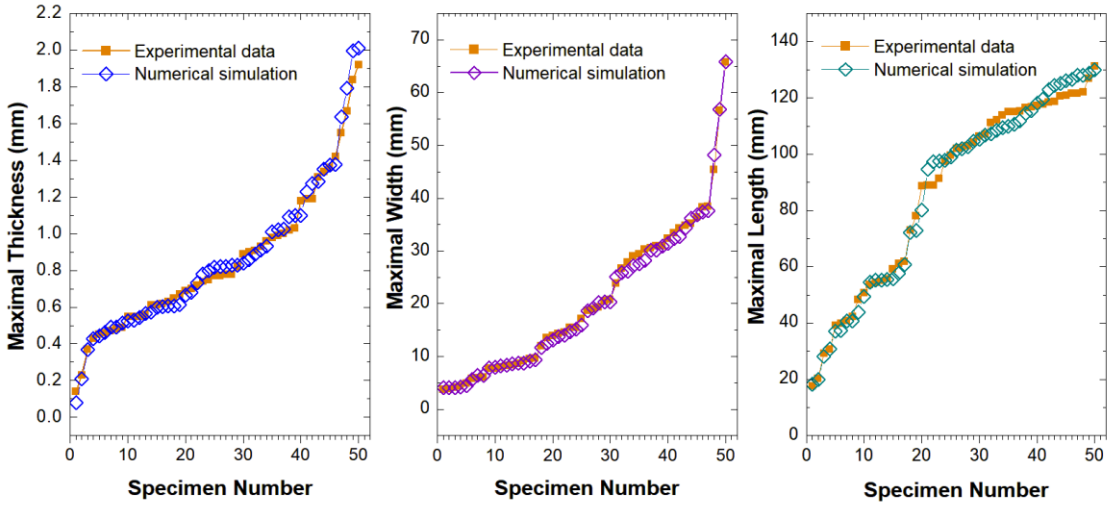

Fig. 12. Comparison of geometric parameters (thickness, length, and width) of disintegrated particles

Of the 50 measurements of particles taken, the deviation in particle length was up to 2% in 3 specimens, and 18 specimens had a deviation of over 15%. The deviation of particles width was up to 2% in 4 specimens, in 15 specimens the deviation was above 15%. The deviation of particles thickness up to 2% was in 21 specimens, in 6 specimens the deviation was above 15%.

Discussion

It is a challenge to establish a comprehensive description of the behavior of spruce wood across various strain rates, ranging from quasi-static to very high strain rates, especially with respect to its anisotropic (orthotropic) properties. As Widehammar (2004) points out, the process of disintegrating wood material into wood chips occurs at elevated

temperatures and very high strain rates of around 10^3 s^{-1}. Standard test devices, such as the Hopkinson split bar (SHPB) (Kruszka and Sobczyk 2022) (Sebek *et al*. 2021), are insufficient to reach these very high strain rates that correspond to industrial applications. The shape and the size of strands are expected to be improved with developments in the geometry of disintegration knives. The need to address this issue is evident from the papers of Nati *et al*. (2010) and Spinelli *et al*. (2014), who confirmed that knife wear resulted in a sharp drop in productivity (>20%) and severe decay in product quality. However, to our best knowledge, there has been almost no follow-up research. There is a need to tackle the topic by a systematic basic research on the effect of chipping knives geometry on the different types of wood material processed, *e.g.*, such as the study on biomass hammer mills (Roy *et al*. 2020). Therefore, the experiment was carried out using the Taylor anvil test device (Jopek 2021), which simulates the production and loading of each strands in real world in industrial practice. The yield strength under quasi-static conditions reaches a value of 10.95 MPa. The value of the hardening coefficient, defined by the general Ludwig-Hollomon equation, was 0.43, and the final strength of the examined spruce wood reached the value of 18.2 MPa. Subsequently, there was a gradual decrease in stress to a value of 4 MPa at a true plastic strain of 0.5. The drop from a true strain value of 0.035 is associated with interfacial failure, particularly along the grain direction of the spruce wood.

From the same spruce wood board used for quasi-static tests, TAT tests were also conducted. As shown in Fig. 4, the specimen underwent a change in its maximum diameter at the impact surface, at the expense of its length. The maximum diameter of the test specimen after the TAT experiment at an impact speed of 144 m/s was 15 mm, and the length of the specimen after the TAT experiment was reduced to 36.5 mm. At the edges of the specimen, there was evident interfacial failure. This fact corresponds to the results of the quasi-static tests, as failure occurred at a true strain of 0.035. In the TAT, the maximum true strain at a speed of 144.5 m/s had a value of 0.76.

The deformation behavior of the specimen was cross-referenced with high-speed camera recordings, as shown in Fig. 5, which indicates that plastic deformation of the test specimen had already occurred at 160.5 m/s. At 60 μs after impact, interfacial failure along the grain direction of the spruce became evident, leading to its separation from the test specimen. The main effect of stress pulses occurred only in the front of the test specimen. To unequivocally demonstrate these results, a stress pulse measurement device was developed and installed, replacing the rigid plate typically used for TAT experiments (Taylor 1948) or the drop tower test (Eakins and Thadhani 2007). From the stress pulse recordings shown in Figs. 6a and 6b, it is evident that there was an initial sharp increase in stress on the rod, followed by a significant decrease and a subsequent increase in stress, which only reached a quarter of the maximum stress peak. In particular, the time at which the maximum stress peak is achieved corresponds, according to the high-speed camera, to the time at which the maximum plastic deformation of the specimen has been reached without noticeable destruction of the specimen. It can be assumed that the maximum plastic deformation is reached, subsequently leading to the ultimate strength, *i.e.*, interfacial failure at the front of the test specimen, without interrupting the internal continuity of the undeformed portion of the test specimen.

The force curves recorded for the test specimens at speeds of 144.5 m/s and 197.6 m/s are shown in Fig.7a and 7b. The character of these curves does not correspond fully to the stress pulse recordings on the rod. Initially, the force reached a local maximum at 29 μs after the first recorded value, followed by a decrease in impact force, and then, at 39 μs after the first recorded value, it reached its maximum again. The duration of the impact

force from the local maximum to a significant drop in force lasted approximately 26 to 30 μs. The difference between the force profile and the stress pulse profile can be explained by the presence of a transient contact area between the test impact rod and the dynamometer's front face. When the contact areas of the rod end with the front face become coherent, the maximum impact force (stress pulse) was transmitted. After converting the maximum stress on the rod to the value of the impact force in the rod, which was generated by the impact of the test specimen on the rod and measured as the maximum force on the dynamometer, it can be concluded that the difference in force magnitudes in the rod and the dynamometer ranged from 2 to 7%, depending on the impact speed of the test specimen. A practical experiment of spruce wood disintegration was conducted on the knife ring flaker and compared with a numerical simulation on the disintegration process. Geometric dimensions (thickness, length, and width) of the disintegrated particles were compared. The differences in the size of disintegrated particles between the measurements and numerical simulations in terms of geometric accuracy were in our opinion due to three aspects:

1. In the random orientation of the feedstock in the knife ring flaker itself. The feedstock is fed into the knife ring flaker *via* a shaker conveyor and subsequently pieces of feedstock are randomly drifted by the rotor knives relative to the static knives in the knife ring flaker, causing random orientation of the feedstock in the disintegration process. By contrast, in the numerical simulation, the orientation is set according to the authors' previous professional experience.
2. In the inherent defects of the feedstock. While in the tests, specimens without defects were selected for larger pieces to be disintegrated, it is not possible to guarantee that natural defects are not present in the feedstock.
3. Inaccurate setting of functional gaps or the effect of wear of the disintegrating knife tool in the knife ring flaker - This aspect is mainly related to the inaccuracy of the measured particle thickness with respect to the numerical simulation, where the disintegrating knives are assumed to have a constant disintegration gap.

Further research will focus on these three aspects. This will involve monitoring the orientation of the feedstock in the knife ring flaker using a high-speed camera including force measurements on the individual static knives of the knife ring flaker and a detailed analysis of the internal natural defects of the feedstock entering the knife ring flaker, as well as measuring the functional geometry and setting the actual geometry and gaps in the disintegration tools.

CONCLUSIONS

1. The results of the optimized numerical simulations of the Taylor anvil test (TAT) for both material models closely matched the experimentally obtained results.
2. Up to a true strain value of 0.035, the parameters of the Johnson-Cook (J-C) model were as follows: A = 10.59 MPa; B = 30.59 MPa; C = 0.01; n = 0.43.
3. Experimentally measured stress pulse profiles on the impact rod corresponded to the stress pulse profiles obtained through numerical simulation for the J-C damage material model.

4. By comparing the experiment and numerical simulation of TAT, parameters for the J-C damage model were determined: D_1 = 0.025; D_2 = 0.197; D_3 = -0.084; D_5 = -0.015; σ_m/σ_{ef} = -9.039
5. From experiments and numerical simulations results, it has been demonstrated that spruce wood does not exhibit negative sensitivity to strain rate.
6. A practical experiment of spruce wood disintegration process was compared with a numerical simulation. The differences can be attributed to three aspects: a) the random disintegration process in the knife ring flaker, b) internal defects of the feedstock, and c) the geometry and precision of knife adjustment, in particular the wearing of the ring knives flaker.

ACKNOWLEDGMENTS

The authors are grateful for the support of the Slovak Research and Development Agency under contracts No. SK-CZ-RD-21-0100 and Ministry of Education, Youth and Sports of the Czech Republic by project No. INTER-EXCELLENCE - LUASK22094.

REFERENCES CITED

Buchar, J., Severa, L., Havlicek, M., and Rolc, S. (2000, September). "Response of wood to the explosive loading," *Journal de physique IV 10*, 529-534. DOI: 10.1051/jp4:2000988

Eakins, D., and Thadhani, N. N. (2007, November). "Analysis of dynamic mechanical behavior in reverse Taylor anvil-on-rod impact tests," *International Journal of Impact Engineering* 34, 1821-1834. DOI:10.1016/j.ijimpeng.2006.11.001

Europe, F. (2020). "State of Europe's forests 2020," Retrieved from https://foresteurope.org/wp-content/uploads/2016/08/SoEF_2020.pdf

Cook,G. R., and Johnson, W. H. (1985). "Fracture characteristics of three metals subjected to various strains, strain rates, temperatures and pressures." *Engineering Fracture Mechanics* 1, pp. 31-48. DOI: 10.1016/0013-7944(85)90052-9

Holmgren, S. E., Svensson, B. A., Gradin, P. A., and Lundberg, B. (2008, September). "An encapsulated split Hopkinson pressure bar for testing of wood at elevated strain rate, temperature, and pressure," *Experimental Techniques* 32, 44-50. DOI:10.1111/j.1747-1567.2008.00318.x

Jopek, M. (2021, August). "Determination of carbon steel dynamic properties," *Manufacturing Technology* 21, 479-482. DOI:10.21062/mft.2021.061

Khare, S., Kumar, K., Choudhary, S., Singh, P. K., Verma, R. K., and Mahajan, P. (2021, December). "Determination of Johnson-Cook material parameters for armour plate using DIC and FEM," *Metals and Materials International* 27, 4984-4995. DOI: 10.1007/s12540-020-00895-3

Kruszka, L., and Sobczyk, K. (2022). "Applications of Hopkinson bar technique for capability testing of high-energy absorption materials," in: *Security Related Advanced Technologies in Critical Infrastructure Protection: Theoretical and Practical Approach*, T. A. Kovacs, Z. Nyikes, and I. Furstner (eds.), pp. 13-27. DOI: 10.1007/978-94-024-2174-3_2

Lipinski, T. (2023, February). "Effect of impurities spacing on fatigue strength coefficient," *Coatings*, 13. DOI: 10.3390/coatings13020242

Moilanen, C. S., Bjorkqvist, T., Engberg, B. A., Salminen, L. I., and Saarenrinne, P. (2016, February). "High strain rate radial compression of Norway spruce earlywood and latewood," *Cellulose* 23, 873-889. DOI: 10.1007/s10570-015-0826-5

Nati, C., Spinelli, R., and Fabbri, P. (2010, May). "Wood chips size distribution in relation to blade wear and screen use," *Biomass and Bioenergy* 34, 583-587. DOI: 10.1016/j.biombioe.2010.01.005

Palamidi, E., and Harrigan, J. J. (2006, August). "An investigation of balsa wood over a range of strain-rates and impact velocities," *Journal de Physique IV* 134, 225-230. DOI: 10.1051/jp4:2006134034

Pettersen, R. C. (1984). "The chemical-composition of wood," *Advances in Chemistry Series*, pp. 57-126.

Roy, S., Lee, K., Lacey, J. A., Thompson, V. S., Keiser, J. R., and Qu, J. (2020, March). "Material characterization-based wear mechanism investigation for biomass hammer mills," *ACS Sustainable Chemistry and Engineering* 8, 3541-3546. DOI: 10.1021/acssuschemeng.9b06450

Sebek, F., Kubik, P., Tippner, J., and Brabec, M. (2021, November). "Orthotropic elastic-plastic-damage model of beech wood based on split Hopkinson pressure and tensile bar experiments," *International Journal of Impact Engineering* 157. DOI: 10.1016/j.ijimpeng.2021.103975

Shin, H.-S., Park, S.-T., Kim, S.-J., Choi, J.-H., and Kim, J.-T. (2008, April). "Deformation behavior of polymeric materials by Taylor impact," *International Journal of Modern Physics B* 22, 1235-1242. DOI: 10.1142/S0217979208046591

Spinelli, R., Glushkov, S., and Markov, I. (2014, March). "Managing chipper knife wear to increase chip quality and reduce chipping cost," *Biomass and Bioenergy* 62, 117-122. DOI: 10.1016/j.biombioe.2014.01.007

Taylor, G. (1948). "The use of flat-ended projectiles for determining dynamic yield stress I. Theoretical considerations," (194), 289–299.

White, B. W., Thadhani, N. N., Jordan, J. L., and Spowart, J. E. (2009). "The effect of particlereinforcement on the dynamic deformation of epoxy-matrix composites," in: *Shock compression of condensed matter - 2009, PTS 1 and 2*, *1195*, M. L. Elert, W. T. Buttler, M. D. Furnish, W. W. Anderson, and W. G. Proud (eds.), pp. 1245+.

Widehammar, S. (2004, February). "Stress-strain relationships for spruce wood: Influence of strain rate, moisture content and loading direction," *Experimental Mechanics* 44, 44-48. DOI: 10.1177/0014485104039748

Yu, M., Wang, B., Ji, P., Li, B., Zhang, L., and Zhang, Q. (2023). "Simulation analysis of the circular sawing process of medium density fiberboard (MDF) based on the Johnson-Cook model," *European Journal of Wood and Wood Products* 82(4). DOI: 10.1007/s00107-023-02007-5

Zulkifli, E., Kusumaningrum, P., and Rahmi, D. P. (2021). "Experimental study and numerical model of spruce and teak wood strength properties under compressive high strain rate loading," *Journal of Engineering and Technological Sciences* 53(1), 85. DOI: 10.5614/j.eng.technol.sci.2021.53.1.3

Article submitted: February 20, 2024; Peer review completed: March 9, 2024; Revised version received and accepted: April 10, 2024; Published: April 25, 2024.
DOI: 10.15376/biores.19.2.3725-3739